

pubs.acs.org/crystal Article

Two Manganese Metalloporphyrin Frameworks Constructed from a Custom-Designed Porphyrin Ligand Exhibiting Selective Uptake of CO₂ over CH₄ and Catalytic Activity for CO₂ Fixation

Published as part of a Crystal Growth and Design virtual special issue on Coordination Polymers as Heterogeneous Catalysts for Water Splitting and CO₂ Fixation

Zachary L. Magnuson, Qigan Cheng, Weijie Zhang, Yu-Sheng Chen, Lukasz Wojtas, Ayman Nafady, Abdullah M. Al-Enizi, Randy W. Larsen, X. Peter Zhang, and Shengqian Ma*



Cite This: *Cryst. Growth Des.* 2021, 21, 2786–2792



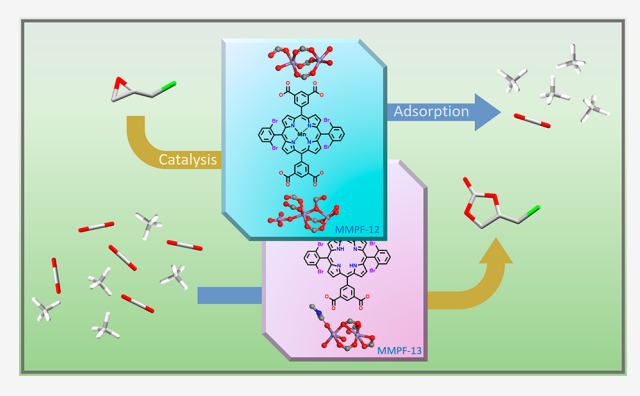
ACCESS

III Metrics & More



s Supporting Information

ABSTRACT: In this work, two new metal-metalloporphyrin frameworks (MMPFs), namely, MMPF-12 and MMPF-13, having unique structural formulas as $[Mn_{24}O_{78}(Mn-dcdbp)_{12}]$ and $[Mn_{8.65}(dcdbp)_8](DMF)_{14}(H_2O)_8$, respectively, were synthesized via the reaction of the custom-designed porphyrin ligand 5,15-bis(3,5-dicarboxyphenyl)-10,20-bis(2,6-dibromophenyl) porphyrin (dcdbp) and hydrated manganese nitrate under solvothermal conditions. Single-crystal X-ray diffraction analysis reveals three-dimensional porous structures with MMPF-12 exhibiting nearly complete metalation of the ligand, whereas MMPF-13, unusually, contains only a small fraction of metalated porphyrin. Gas sorption studies attest to a permanent porosity together with selective adsorption of CO_2 over CH_4 . Additionally, both MMPFs catalyzed CO_2 cycloaddition of



electronically and sterically substituted epoxide substrates, thereby providing access to important products under mild conditions. Results also showed that the ligand-metalated MMPF-12, containing trimer Mn clusters, has a higher catalytic activity than its congener MMPF-13, which has only dimer clusters. Thus, Mn clusters likely play an important role in both the structure of the MMPFs and their activity toward the transformation of CO_2 , with the enhanced catalytic activity being ascribed to the conserved porous structure.

■ INTRODUCTION

Metal—organic frameworks (MOFs) are a class of crystalline solids defined by their versatile porosity and bespoke construction of organic ligands (linkers), which connect metallic nodes, also known as secondary building units (SBUs), into a lattice structure. The incredible flexibility of design found in organic ligands paired with the highly modal binding through SBUs in MOFs has spurred research activities focused on these diverse materials. These endeavors have produced exceptional understanding and precise control of the intrinsic physical characteristics such as porosity and stability, as well as functionalization toward applications in sensing, separations, gas sorption, catalysis, nonlinear optics, biomedical imaging, and drug delivery. 1—4

Relevant to the present work are porphyrins and metalloporphyrins, which are unique, naturally occurring macrocycles that serve as the basis for a variety of linkers. Owing to their intriguing electronic, photochemical, and catalytic properties,^{5–9} these compounds have been synthesized and implemented in various applications including functional catalytic sites in biological systems. However, the notorious synthesis of porphyrinic materials has, to some extent, restricted their use to simple molecules or commercially available ones, particularly in MOF research. Virtually, the synthesis of new porphyrin-based linkers for the preparation of porphyrin-containing MOFs, or metal-metalloporphyrin frameworks (MMPFs), will inevitably produce novel materials with exceptional topologies and physical characteristics. Therefore, this is a key route toward the evolution of MMPF research. MMPFs allow for the heterogenization of porphyrin catalysts, which by design remedies the significant drawbacks of homogeneous porphyrin catalysis such as aggregation and

Received: December 16, 2020 Revised: April 2, 2021 Published: April 19, 2021





destructive self-oxidation (both of which can seriously hamper catalytic efficacy), ^{16,17} along with the necessary separation of otherwise homogeneous catalysts from the reaction mixture. In addition to the proposed facile separations, these catalysts can be easily recycled and used multiple times without significant decay in performance or leeching of structural components. ^{18,19} The choice of manganese for the synthesis of these MMPFs is based on the great diversity of topologies possible as well as for its functionality in the targeted catalysis reaction. ^{20,21}

Recent reports of Mn-based MOFs functioning as CO2 cycloaddition catalysts, including a one-pot transformation of olefins into cyclic carbonates utilizing an imidazolium bromide functionalized MOF²² and a visible-light-assisted cycloaddition,²³ provide valuable insight into designing systems that offer novel means to a similar end. Though MMPF-12 and -13 affect high efficiencies with relatively low catalyst loading and mild conditions, a comparison is warranted. In the former work, considering only the conversion of styrene oxide to styrene carbonate, a much higher ratio of catalyst and cocatalyst is required at higher pressure and temperature to affect yields like those observed with MMPF-12 and -13, in a quarter of the time. In the latter work, a more rigid comparison is drawn as substrate and cocatalyst are identical: under ambient temperature and 1 atm with additional catalyst loading (and less cocatalyst) complete conversion of epichlorohydrin is achieved in the same amount of time, this result being clearly attributed in some part to the light used. Additionally, comparisons are drawn between several heterogeneous catalysts, including MOFs, for cycloaddition of CO2 to epoxides in a review by Marciniak et al.²⁴

Recent statistics in 2018 have revealed that carbon dioxide (CO₂) emission has accounted for 81% of greenhouse gases. Though it is sequestered naturally in several environmental compartments, these sinks have not kept up with changes in anthropogenic emission, leading to an overall increase in atmospheric CO₂. ²⁵ Carbon capture through the chemical fixation of CO2 is an appealing approach in addressing and mending the environmental impact of anthropogenic CO2 emission, particularly, conversion of CO2 into useful compounds, thereby adding economic value for the byproducts of sequestration. 26,27 This can be achieved effectively through the application of MMPFs toward the catalytic cycloaddition of CO₂ to epoxides, yielding dioxolanones, which are a class of compounds utilized in polycarbonate materials, electrolytes in lithium batteries, pharmaceutical production, antifungal agents, and as polar solvents.²⁸⁻³

In view of these demanding challenges and as a continuation of our interest in the MOFs research, we offer in this contribution a facile approach for the synthesis and detailed structural characterization of two manganese-based MMPFs, namely, MMPF-12 and MMPF-13, and their applications in both selective ($\rm CO_2/CH_4$) gas sorption and catalytic cycloaddition of $\rm CO_2$ to epoxides as an access to a series of important compounds.

■ EXPERIMENTAL SECTION

With slight modification of the solvents and temperature used in the syntheses, two porous porphyrinic manganese MMPFs, denoted as MPPF-12 and MPPF-13, were obtained. MMPF-12 was synthesized via a hydrothermal method using $Mn(NO_3)_2\cdot 4H_2O$ (0.28 mmol), (H₄dcdbp, Figure 1) (0.002 mmol), dimethylacetamide (DMA) (0.009 mmol), methanol (0.005 mmol), and water (3.7 mmol). After

Figure 1. Porphyrin ligand that serves as the organic linker in MMPF-12 and MMPF-13:5,15-bis(3,5-dicarboxyphenyl)-10,20-bis(2,6-dibromophenyl)porphyrin (H₄dcdbp).

three days, deep purple crystals of MMPF-12 were isolated in 58% yield based on the Mn. MMPF-13 was prepared in a similar manner as that of MMPF-12 with the exception of DMA being replaced by *N,N*-dimethylformamide (DMF) and methanol with ethanol. The modified reaction produced purple crystals of MMPF-13 in 54% yield based on Mn.

Single-crystal X-ray diffraction analysis revealed that compound MMPF-12 crystallizes in the orthorhombic space group Pnma. Manganese seated in the porphyrin core with a near-perfect tetrahedral $\{N_4\}$ geometry, coordinating with the four nitrogen atoms of dcdbp exhibiting a (III) oxidation state based on spectral analysis (Figure S1). Additionally, the metal center appears to possess trans-axial ligation of one hydroxo group and one solvent molecule (DMA, methanol, or water) based on single-crystal X-ray diffraction data. The length of Mn-N bonds range from 1.9730 to 2.0970 Å. MMPF-12 exhibits one Mn₂O₃(CO₂)₄ dimer secondary building unit (SBU) and two isostructural Mn₃O₅(HCO₂⁻)(CO₂)₄ trimer SBUs. As presented in Figure 2, in the dimer SBUs, Mn1 ions coordinate with five oxygen atoms from three bidentate bridging μ_2 - $\eta_1\eta_1$ carboxylates and two water molecules with a square pyramidal geometry. Mn2 ions exhibit the same geometry as Mn1; yet, Mn2 ions are instead coordinated with three carboxylate groups from three different dcdbp ligands, one μ_1 - η_1 carboxylate, and one OH group. Consequently, two pentacoordinated Mn atoms linked by three μ_2 - $\eta_1\eta_1$ carboxylate groups construct the dimer SBUs. Three crystallographically distinct Mn ions could be observed in the Mn₃O₅(HCO₂⁻)(CO₂)₄ trimer. In the trimer SBUs, Mn4 is surrounded by six oxygen atoms from two bidentate bridging μ_2 - $\eta_1\eta_1$ carboxylates, two $\mu_1\text{-}\eta_1$ carboxylates, a water molecule, and oxygen from HCO2-. Mn5 is coordinated with two carboxylate oxygen atoms, one HCO₂ group, and two oxygen atoms to complete a square pyramidal geometry. Importantly, as shown in Figure 2, the difference between two Mn₃O₅(HCO₂⁻)(CO₂)₄ trimers was that Mn6 connected by an oxygen atom as well as two μ_2 - $\eta_1\eta_1$ carboxylates. Further structural analysis revealed that all of the nodes in the structure of MMPF-12 are 4-connected; thus, MMPF-12 exhibits an nbo topology.

Single-crystal X-ray diffraction analysis revealed that MMPF-13 crystallizes in the orthorhombic space group Pbca. The low occupancy (determined by analysis of XRD data to be about 92% freebase) of Mn in the porphyrin macrocycle indicates that the linker is primarily a freebase porphyrin. Interestingly, the dihedral angles between the porphyrin plane and the attached dicarboxylate benzene rings are different, 58.9 and 65.6 deg. The ligand dcdbp in this case exhibits multimodal coordination. The asymmetric unit of MMPF-13 consists of two crystallographically unique Mn ions. Mn1 is fully coordinated to the dcdbp ligand with seven oxygen atoms from one bridging μ_2 - $\eta_2\eta_1$ carboxylate, one bidentate bridging μ_2 - $\eta_1\eta_1$ carboxylate, one μ_1 - η_1 carboxylate, and three oxygen atoms from free water molecules and an OH group. Mn2 is coordinated with five oxygen atoms from two bidentate bridging μ_2 - $\eta_1\eta_1$ carboxylates, two water molecules, and one oxygen from DMF.

Crystal Growth & Design pubs.acs.org/crystal Article

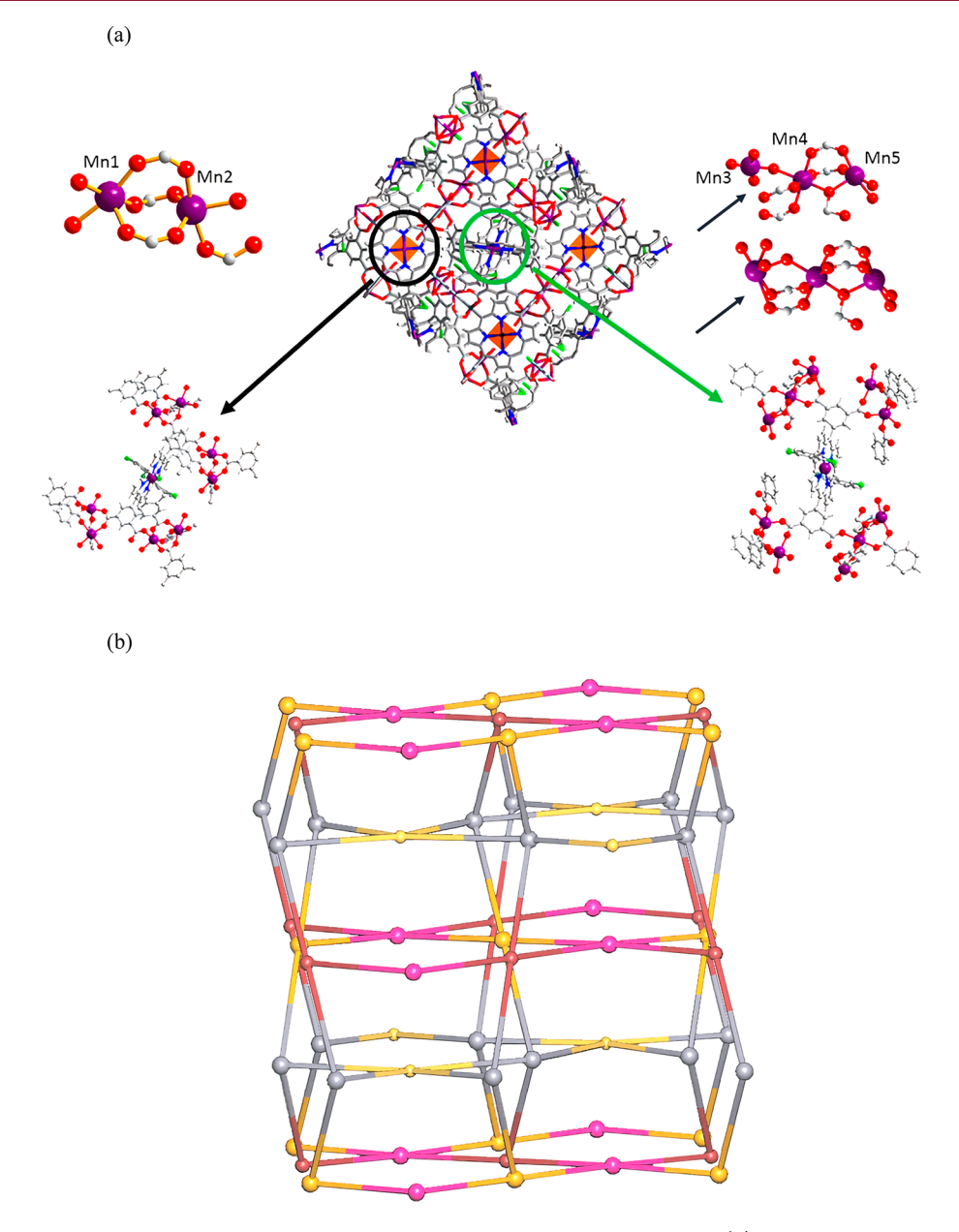


Figure 2. (a) View of the open-framework structure of MMPF-12 along the crystallographic c axis. (b) Topological view of MMPF-12 where the colors hot pink, salmon, gray, and yellow nodes represent the trimetallic Mn SBU, the dioxo Mn(III) dcdbp with biaxially coordinated DMA, the bimetallic Mn SBU, and the dioxo Mn(III) dcdbp without crystallographically resolved coordination at the axial positions, respectively.

As expected, the $\rm Mn_2O_2(DMF)(CO_2)_4$ SBUs serves as a 4-connected node with the organic linker, which is also a 4-connected node, constructing the framework of MMPF-13. As shown in Figure 4, MMPF-13 exhibits a 4-connected **nbo** topological structure.

As shown in Figure S3a, the powder X-ray diffraction (XRD) patterns of the MMPF-12 reveal an inferior crystallinity when compared to the simulated pattern, presumably due to partial framework collapse upon the removal solvent. This could also be attributed to the inherent nature of porphyrinic frameworks degrading when undergoing XRD analysis as a result of strong background X-ray fluorescence.³¹ The overall XRD pattern of MMPF-13 was in good agreement with the simulated pattern. Thermogravimetric analysis (TGA) of MMPF-12 indicated that moderate weight loss occurred at elevated temperatures (Figure S4a). It was also found that a sharp weight loss of over 24% was observed as the temperature was increased from 400 to 700 °C, thereby suggesting a thermal decomposition of MMPF-12 in that temperature range. Furthermore, MMPF-13 exhibited similar thermal decomposition as shown in Figure S4b.

For gas sorption studies, MMPF-12 was activated using supercritical $\rm CO_2$ due to its sensitivity to solvent evacuation, preserving its porous structure for analysis. At 273 and 298 K (Figure S6 and Figure S7), MMPF-12 exhibited much higher sorption selectivity for $\rm CO_2$ than $\rm CH_4$. As shown in Figure 5, MMPF-12 adsorbed 49 cm³/g $\rm CO_2$ at 1 atm and 273 K, with $\rm CH_4$ adsorption being much lower. This high selectivity and moderate sorption capacity are crucial parameters for applications in gas separation. The significant selectivity for $\rm CO_2$ is most likely due to electrostatic pore—surface interactions brought on by the quadrupole moment of $\rm CO_2$, which $\rm CH_4$ does not possess. Additionally, $\rm CO_2$ is smaller than $\rm CH_4$, which can attest to the overall difference in uptake values.

To investigate the gas storage capacity of MMPF-13, CO₂ and CH₄ sorption was measured at near-ambient temperature. Differing from MMPF-12, MMPF-13 showed a considerably lower selectivity for CO₂ over CH₄ at 273 and 298 K (Figure 6 and Figure S7). At 1 atm of pressure, the CO₂ uptakes were 34 cm³/g at 273 K and 23 cm³/g at 298 K. For comparison, the CH₄ uptakes were only 12 cm³/g at 273 K and 6 cm³/g at 298 K.

Crystal Growth & Design pubs.acs.org/crystal Article

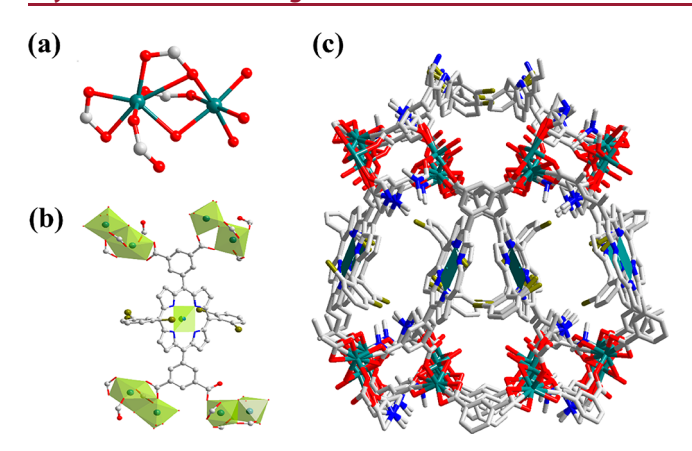


Figure 3. (a) The dinuclear Mn cluster in MMPF-13; (b) the connected style of the porphyrin ligand; (c) perspective view of the open-framework structure of MMPF-13.

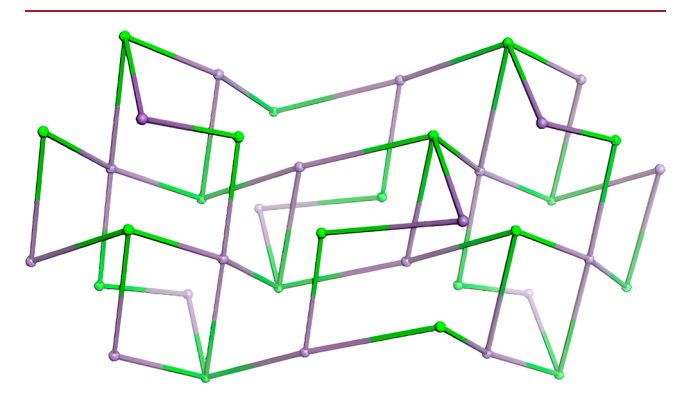


Figure 4. Topological structure of MMPF-13, where the colors lime and gray represent the bimetallic Mn SBU and the primarily freebase dcdbp, respectively.

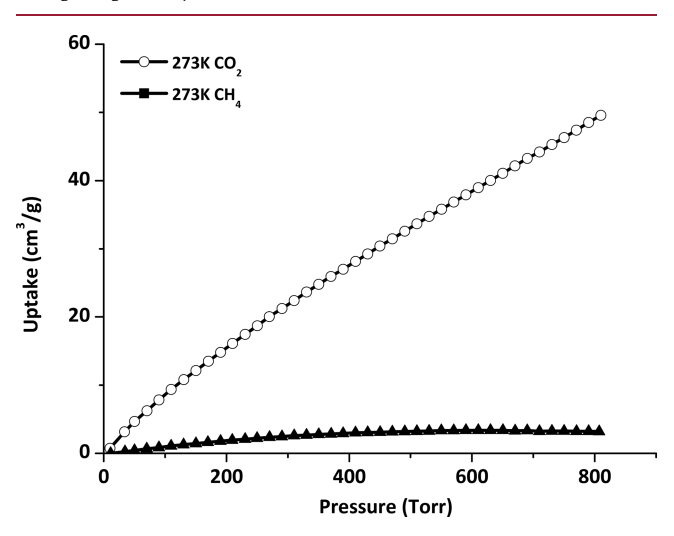


Figure 5. Gas sorption isotherms of MMPF-12 for $\mathrm{CH_4}$ and $\mathrm{CO_2}$ at 273 K.

Isosteric heat of adsorption was calculated to better characterize the observed CO₂ uptakes. As shown in Figure 7a, the adsorption enthalpy of MMPF-12 is much higher than that of MMPF-13, indicating stronger interactions between the CO₂ molecules and the host framework, noting that MMPF-13 contains almost entirely freebase dcdbp. To estimate the practical separations capability for CO₂, an IAST plot of gas mixtures of CO₂/CH₄ (50/50%) was considered, a common method to predict binary mixture adsorption from experimental single-component isotherms. As shown in Figure

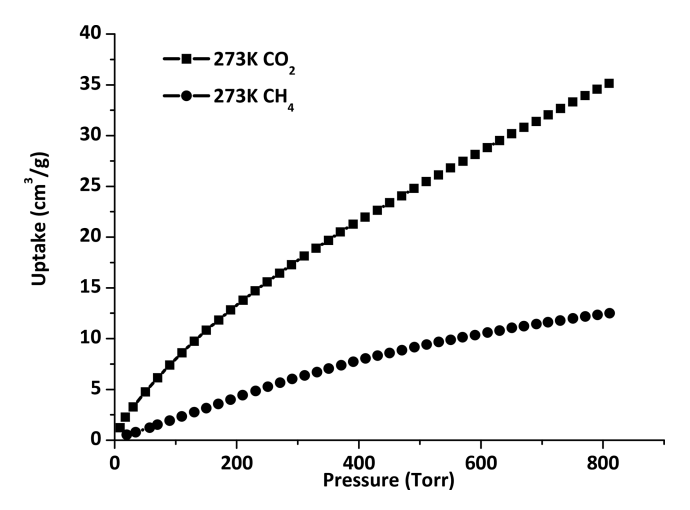
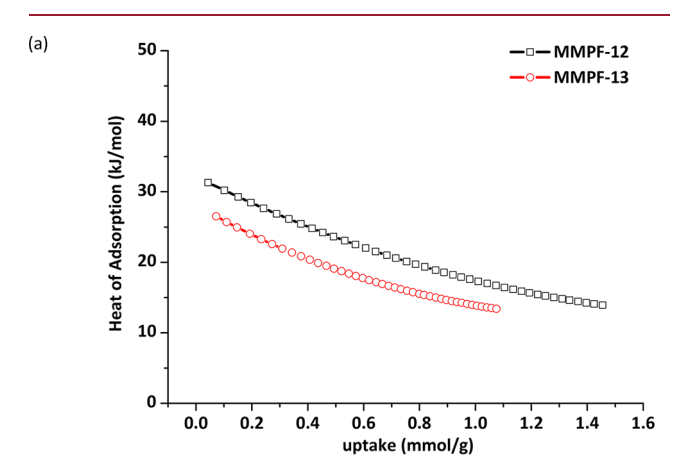


Figure 6. Gas sorption isotherms of MMPF-13 for CH_4 and CO_2 at 273 K.



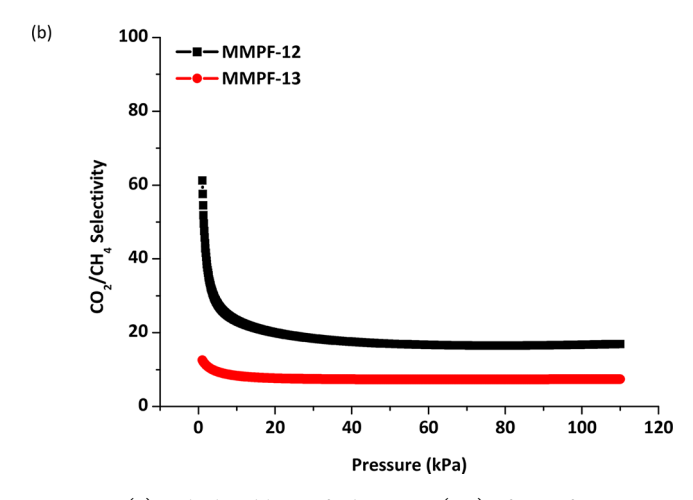


Figure 7. (a) Calculated heat of adsorption ($Q_{\rm st}$) of CO₂ for MMPF-12 and MMPF-13. (b) Gas mixture adsorption selectivities were predicted by IAST at 298 K and 100 kPa for MMPF-12 and MMPF-13.

7b, at 298 K and 1 bar, the selectivity of $\rm CO_2$ over $\rm CH_4$ for MMPF-12 and MMPF-13 according to the experimental data is 61 and 13 at 298 K and 1 bar, respectively.

Increased pore sizes in MMPF-13 led to a reduced molecular sieving effect, as well as the absence of Mn-metalated porphyrin,

Table 1. Conversion Efficiencies for MMPF-12 and MMPF-13^a

MMPF-12 & 13 Catalyzed Addition of CO₂ to Epoxides

Entry	Substrate	Product	MMPF-12 Yield	MMPF-13 Yield
1	CI	CI	98% ±1%	89% ±2%
2	٥		89% ±2%	77% ±3%
3			85% ±3%	65% ±2%

[&]quot;Reactions of 6.3 mmol of epoxide, 0.08 mmol of TBAB, and 2 mg (3 wt %) of MMPF catalyst were performed under 1 atm of CO_2 at 40 °C for 24 h.

which could serve as a good binding site for CO_2 but did not function similarly for CH_4 . Both could be in part responsible for the difference in selectivity observed.

CO₂ cycloaddition of several epoxides catalyzed by MMPF-12 and MMPF-13 in the presence of cocatalyst tetra-butylammonium bromide (TBAB) was performed under mild conditions using epichlorohydrin as the model compound. Detailed reaction conditions are described in Supporting Information. After each reaction, ¹H NMR was performed directly on the centrifuged reaction solution to determine the percent yield of the product. On the basis of these conversions (Table 1), MMPF-12 outperformed MMPF-13 for each epoxide tested, with the decrease in product yield trend possibly being caused by the change in the size of the substrate, which could restrict diffusion through the pores of the MMPFs, thus reducing the interaction between substrate and the bulk of the catalysts.³² It is worth noting that the performance of MMPF-12 relative to MMPF-13 could also result from the difference in the porphyrin linkers. As mentioned earlier, MMPF-12 exhibits complete metalation of the porphyrin ligand, while the metalation in MMPF-13 is negligible. The fact that MMPF-13 performed these reactions with similar efficiency despite having less Mn per mole of material suggests that the SBUs of MMPF-13 and likely those of MMPF-12 may be functioning as catalytic centers. Additionally, binuclear nodes occur in both materials, while trinuclear nodes are only present in MMPF-12. The trinuclear nodes exhibit an open manganese center and as a result may possess a remarkable catalytic activity.



Figure 8. Schematic representation of catalytic ${\rm CO_2}$ cycloaddition to an epoxide.

CONCLUSION

In summary, two manganese MMPFs were constructed under solvothermal conditions utilizing the ligand H_4 dcdbp. Both MMPF-12 and MMPF-13 showed relatively high thermal stability, good catalytic activity, enhanced adsorption capacity, and efficient selectivity for CO_2 over CH_4 . Ultimately, the combined findings of this work make MMPF-12 and MMPF-13 potential candidates for environmental applications, emphasizing that the inherent value of greenhouse gases does not have to be lost in the remediation process.

ASSOCIATED CONTENT

Supporting Information

The Supporting Information is available free of charge at https://pubs.acs.org/doi/10.1021/acs.cgd.0c01694.

Materials and crystallographic methods, crystal data refinement, representative synthesis of crystals and cycloaddition reactions, PXRD of pristine crystals and postreaction, NMR, and FT-IR spectra, TGA, and gas sorption isotherms (PDF)

Accession Codes

CCDC 2051320 and 2051331 contain the supplementary crystallographic data for this paper. These data can be obtained free of charge via www.ccdc.cam.ac.uk/data_request/cif, or by emailing data_request@ccdc.cam.ac.uk, or by contacting The Cambridge Crystallographic Data Centre, 12 Union Road, Cambridge CB2 1EZ, UK; fax: +44 1223 336033.

AUTHOR INFORMATION

Corresponding Author

Shengqian Ma — Department of Chemistry, University of South Florida, Tampa, Florida 33620, United States; Department of Chemistry, University of North Texas, Denton, Texas 76201, United States; orcid.org/0000-0002-1897-7069; Email: Shengqian.Ma@unt.edu

Authors

Zachary L. Magnuson – Department of Chemistry, University of South Florida, Tampa, Florida 33620, United States

Qigan Cheng – Department of Chemistry, University of South Florida, Tampa, Florida 33620, United States

Weijie Zhang – Department of Chemistry, University of North Texas, Denton, Texas 76201, United States

Yu-Sheng Chen – ChemMatCARS, Center for Advanced Radiation Sources, The University of Chicago, Argonne, Illinois 60439, United States

Lukasz Wojtas — Department of Chemistry, University of South Florida, Tampa, Florida 33620, United States Ayman Nafady — Department of Chemistry, College of Science, King Saud University, Riyadh 11451, Saudi Arabia

- Abdullah M. Al-Enizi Department of Chemistry, College of Science, King Saud University, Riyadh 11451, Saudi Arabia; orcid.org/0000-0002-3967-5553
- Randy W. Larsen Department of Chemistry, University of South Florida, Tampa, Florida 33620, United States;
 orcid.org/0000-0002-5179-4635
- X. Peter Zhang Department of Chemistry, University of South Florida, Tampa, Florida 33620, United States; Department of Chemistry, Boston College, Chestnut Hill, Massachusetts 02467, United States; orcid.org/0000-0001-7574-8409

Complete contact information is available at: https://pubs.acs.org/10.1021/acs.cgd.0c01694

Notes

The authors declare no competing financial interest.

ACKNOWLEDGMENTS

This work was supported by the U.S. National Science Foundation (DMR-1352065). Partial support from the Robert A. Welch Foundation (B-0027) (S.M.) and Researchers Supporting Program Project No. RSP-2021/79 at King Saud University, Riyadh, Saudi Arabia, is also acknowledged. NSF's ChemMatCARS Sector 15 is supported by the Divisions of Chemistry (CHE) and Materials Research (DMR), National Science Foundation, under Grant Number NSF/CHE-1834750. Use of the Advanced Photon Source, an Office of Science User Facility operated for the U.S. Department of Energy (DOE) Office of Science by Argonne National Laboratory, was supported by the U.S. DOE under Contract No. DE-AC02-06CH11357.

■ REFERENCES

- (1) Furukawa, H.; Cordova, K. E.; O'Keeffe, M.; Yaghi, O. M. The Chemistry and Applications of Metal-Organic Frameworks. *Science* **2013**, *341* (6149), 1230444.
- (2) Wang, C.; Zhang, T.; Lin, W. B. Rational Synthesis of Noncentrosymmetric Metal-Organic Frameworks for Second-Order Nonlinear Optics. *Chem. Rev.* **2012**, *112* (2), 1084–1104.
- (3) Zou, C.; Wu, C.-D. Functional porphyrinic metal—organic frameworks: crystal engineering and applications. *Dalton Trans.* **2012**, 41 (14), 3879–3888.
- (4) Pereira, C. F.; Simões, M. M. Q.; Tomé, J. P. C.; Almeida Paz, F. A. Porphyrin-Based Metal-Organic Frameworks as Heterogeneous Catalysts in Oxidation Reactions. *Molecules* **2016**, *21* (10), 1348.
- (5) Lu, H.; Zhang, X. P. Catalytic C–H functionalization by metalloporphyrins: recent developments and future directions. *Chem. Soc. Rev.* **2011**, 40 (4), 1899–1909.
- (6) Barona-Castaño, J. C.; Carmona-Vargas, C. C.; Brocksom, T. J.; De Oliveira, K. T. Porphyrins as Catalysts in Scalable Organic Reactions. *Molecules* **2016**, *21* (3), 310.
- (7) Birel, O.; Nadeem, S.; Duman, H. Porphyrin-Based Dye-Sensitized Solar Cells (DSSCs): a Review. J. Fluoresc. 2017, 27 (3), 1075–1085.
- (8) Huang, H.; Song, W.; Rieffel, J.; Lovell, J. F., Emerging applications of porphyrins in photomedicine. *Front. Phys.* **2015**, *3*, 23. DOI: 10.3389/fphy.2015.00023
- (9) Pietrzak, M. Porphyrins and metalloporphyrins in electroanalytical chemistry. *Adv. Chem. Res.* **2017**, *36*, 95–152.
- (10) Zou, C.; Zhang, T.; Xie, M.-H.; Yan, L.; Kong, G.-Q.; Yang, X.-L.; Ma, A.; Wu, C.-D. Four Metalloporphyrinic Frameworks as Heterogeneous Catalysts for Selective Oxidation and Aldol Reaction. *Inorg. Chem.* **2013**, *52* (7), 3620–3626.

- (11) Xie, M.-H.; Yang, X.-L.; Wu, C.-D. A metalloporphyrin functionalized metal—organic framework for selective oxidization of styrene. *Chem. Commun.* **2011**, 47 (19), 5521–5523.
- (12) Gao, W.-Y.; Wojtas, L.; Ma, S. A porous metal-metal-loporphyrin framework featuring high-density active sites for chemical fixation of CO2 under ambient conditions. *Chem. Commun.* **2014**, *50* (40), 5316–5318.
- (13) Gao, W.-Y.; Chrzanowski, M.; Ma, S. Metal—metalloporphyrin frameworks: a resurging class of functional materials. *Chem. Soc. Rev.* **2014**, 43 (16), 5841–5866.
- (14) Meng, L.; Cheng, Q.; Kim, C.; Gao, W.-Y.; Wojtas, L.; Chen, Y.-S.; Zaworotko, M. J.; Zhang, X. P.; Ma, S. Crystal Engineering of a Microporous, Catalytically Active fcu Topology MOF Using a Custom-Designed Metalloporphyrin Linker. *Angew. Chem., Int. Ed.* **2012**, *51* (40), 10082–10085.
- (15) Huh, S.; Kim, S.-J.; Kim, Y. Porphyrinic metal—organic frameworks from custom-designed porphyrins. *CrystEngComm* **2016**, 18 (3), 345–368.
- (16) Groves, J. T. Using push to get pull. Nat. Chem. 2014, 6 (2), 89-91.
- (17) Zhao, M.; Ou, S.; Wu, C.-D. Porous Metal-Organic Frameworks for Heterogeneous Biomimetic Catalysis. *Acc. Chem. Res.* **2014**, *47* (4), 1199–1207.
- (18) Cui, H.; Wang, Y.; Wang, Y.; Fan, Y.-Z.; Zhang, L.; Su, C.-Y. A stable and porous iridium(iii)-porphyrin metal—organic framework: synthesis, structure and catalysis. *CrystEngComm* **2016**, *18* (12), 2203–2209.
- (19) Wang, Y.; Cui, H.; Zhang, L.; Su, C.-Y. An Acid Stable Metal-Organic Framework as an Efficient and Recyclable Catalyst for the O–H Insertion Reaction of Carboxylic Acids. *ChemCatChem* **2018**, *10* (17), 3901–3906.
- (20) Gu, J.-Z.; Kirillov, A. M.; Wu, J.; Lv, D.-Y.; Tang, Y.; Wu, J.-C. Synthesis, structural versatility, luminescent and magnetic properties of a series of coordination polymers constructed from biphenyl-2,4,4′-tricarboxylate and different N-donor ligands. *CrystEngComm* **2013**, *15* (47), 10287–10303.
- (21) Gu, J.-Z.; Liang, X.-X.; Cai, Y.; Wu, J.; Shi, Z.-F.; Kirillov, A. M. Hydrothermal assembly, structures, topologies, luminescence, and magnetism of a novel series of coordination polymers driven by a trifunctional nicotinic acid building block. *Dalton Trans.* **2017**, *46* (33), 10908–10925.
- (22) Yu, K.; Puthiaraj, P.; Ahn, W.-S. One-pot catalytic transformation of olefins into cyclic carbonates over an imidazolium bromide-functionalized Mn(III)-porphyrin metal—organic framework. *Appl. Catal., B* **2020**, 273, 119059.
- (23) Sharma, N.; Dhankhar, S. S.; Nagaraja, C. M. A Mn(II)-porphyrin based metal-organic framework (MOF) for visible-light-assisted cycloaddition of carbon dioxide with epoxides. *Microporous Mesoporous Mater.* **2019**, 280, 372–378.
- (24) Marciniak, A. A.; Lamb, K. J.; Ozorio, L. P.; Mota, C. J. A.; North, M. Heterogeneous catalysts for cyclic carbonate synthesis from carbon dioxide and epoxides. *Curr. Opin. Green Sustain. Chem.* **2020**, 26, 100365.
- (25) Inventory of U.S. Greenhouse Gas Emissions and Sinks: 1990–2018; U.S. Environmental Protection Agency, 2020.
- (26) Dalpozzo, R.; Della Ca', N.; Gabriele, B.; Mancuso, R. Recent Advances in the Chemical Fixation of Carbon Dioxide: A Green Route to Carbonylated Heterocycle Synthesis. *Catalysts* **2019**, 9 (6), 511.
- (27) Webster, D. C. Cyclic carbonate functional polymers and their applications. *Prog. Org. Coat.* **2003**, *47* (1), 77–86.
- (28) Deenadayalan, M. S.; Sharma, N.; Verma, P. K.; Nagaraja, C. M. Visible-Light-Assisted Photocatalytic Reduction of Nitroaromatics by Recyclable Ni(II)-Porphyrin Metal—Organic Framework (MOF) at RT. *Inorg. Chem.* **2016**, *55* (11), 5320–5327.
- (29) Li, T.-X.; Yang, M.-H.; Wang, X.-B.; Wang, Y.; Kong, L.-Y. Synergistic Antifungal Meroterpenes and Dioxolanone Derivatives from the Endophytic Fungus Guignardia sp. *J. Nat. Prod.* **2015**, 78 (11), 2511–2520.

- (30) Chai, J.; Liu, Z.; Zhang, J.; Sun, J.; Tian, Z.; Ji, Y.; Tang, K.; Zhou, X.; Cui, G. A Superior Polymer Electrolyte with Rigid Cyclic Carbonate Backbone for Rechargeable Lithium Ion Batteries. *ACS Appl. Mater. Interfaces* **2017**, *9* (21), 17897–17905.
- (31) Klug, H. P.; Alexander, L. E. X-Ray Diffraction Procedures: For Polycrystalline and Amorphous Materials, 2nd ed; Wiley, 1974; p 992.
- (32) Gao, W.-Y.; Tsai, C.-Y.; Wojtas, L.; Thiounn, T.; Lin, C.-C.; Ma, S. Interpenetrating Metal–Metalloporphyrin Framework for Selective CO2 Uptake and Chemical Transformation of CO2. *Inorg. Chem.* **2016**, *55* (15), 7291–7294.